Diffuse Synchrotron Emission Associated with the Starburst in the Circumnuclear Disk of NGC 1275

H. Nagai[1,2] and N. Kawakatu[3]

[1] National Astronomical Observatory of Japan, Osawa 2-21-1, Mitaka, Tokyo 181-8588, Japan; hiroshi.nagai@nao.ac.jp
[2] The Graduate University for Advanced Studies, SOKENDAI, Osawa 2-21-1, Mitaka, Tokyo 181-8588, Japan
[3] National Institute of Technology, Kure College, 2-2-11, Agaminami, Kure, Hiroshima, 737-8506, Japan

Abstract

Recent Atacama Large Millimeter/submillimeter Array (ALMA) observations found a positive correlation between the mass of dense molecular gas in the circumnuclear disks (CNDs) and accretion rate to the active galactic nuclei (AGNs). This indicates that star formation activity in the CNDs is essential for triggering the accretion of mass to AGNs. Although the starburst-driven turbulence is a key mechanism for the transfer of angular momentum and the resultant mass accretion from the CND scale to the inner radius, the observational evidence is lacking. We report the very-long-baseline-interferometry detection of the diffuse synchrotron emission on a scale of several tens of parsecs coinciding spatially with the molecular gas disk recently discovered by ALMA observations in NGC 1275. The synchrotron emissions most likely resulted from the relativistic electrons produced by the supernova explosions. This is unambiguous evidence of the star formation activity in a CND. The turbulent velocity and the scale height of the CND predicted from the supernova-driven turbulence model agree with the observations, although the model-predicted accretion rate disagrees with the bolometric luminosity. This might indicate that additional mechanisms to enhance the turbulence are required for the inner disk. We discuss the multiphase nature of the CND by combining the information of the CO emission, synchrotron emission, and free–free absorption.

Unified Astronomy Thesaurus concepts: Low-luminosity active galactic nuclei (2033); Radio active galactic nuclei (2134); Radio galaxies (1343); Perseus Cluster (1214); Galaxy accretion disks (562); Radio interferometry (1346); Very long baseline interferometry (1769)

1. Introduction

Recent Atacama Large Millimeter/submillimeter Array (ALMA) observations have revealed the presence of massive molecular gas around active galactic nuclei (AGNs). Dozens of sources show a disk-like structure (i.e., so-called circumnuclear disk, hereafter CND) decoupled, both morphologically and kinematically, from the extended galactic-scale molecular gas (e.g., Imanishi et al. 2018; Izumi et al. 2018; Combes et al. 2019). There is a positive correlation between the mass of dense molecular gas in CNDs and AGN accretion rates (Izumi et al. 2016). This suggests that these molecular CNDs are important components to understand the accretion physics in AGNs.

The angular momentum transfer mechanism that enhances the mass accretion from the CND scale to the inner radius has been a subject of discussion. One plausible explanation is that gas turbulence generated by supernova (SN) explosions in the CNDs/tori (i.e., so-called SN-driven turbulence model) has a major role for the transfer of angular momentum (Kawakatu & Wada 2008). However, there has been a lack of direct observational evidence of the star formation activity in the CNDs/tori. Polycyclic aromatic hydrocarbons (PAHs) are widely used as tracers of star formation (e.g., Peeters et al. 2004), but PAHs in the CNDs/tori can be dissociated by harsh AGN radiation. Instead, synchrotron radiation from relativistic electrons produced by SN explosions can be an alternative tracer. For this to be possible, spatially resolved imaging is critical to study the spatial association of the synchrotron emission with molecular CND/tori and decouple the emission from the AGN jets.

NGC 1275 ($z = 0.01755$) is a nearby radio galaxy/giant elliptical galaxy at the center of the Perseus cluster. The radio source of NGC 1275 is also known as 3C 84 and shows multiple radio lobes on different angular scales (Silver et al. 1998; Walker et al. 2000; Nagai et al. 2010). This galaxy is a reservoir of a large amount of cold gas ($M_{gas} \sim 10^9 M_\odot$: Lim et al. 2008; Salomé et al. 2008). On kiloparsec scales, molecular gas filaments are aligned in the east–west direction (Lim et al. 2008) and these filaments seem to coincide with the Hα nebulae (Fabian et al. 2008). Within 100 pc, recent ALMA observations detected a rotating CND with the CO(2−1), HCN (3−2), and HCO$^+$(3−2) lines (Nagai et al. 2019). Intriguingly, the detection of diffuse synchrotron emission on this spatial scale was previously reported by very long baseline interferometry (VLBI) observations at frequencies $\lesssim 1$ GHz (Silver et al. 1998). Both relativistic electrons diffused out from the AGN and those produced by the SN explosions were discussed as origins of the diffuse synchrotron emission, but the actual origin was unclear because of the lack of molecular CND information at that time.

Here we report the detailed comparison of the molecular CND with the diffuse synchrotron emission. Throughout this paper, we used $H_0 = 69.6$, $\Omega_M = 0.286$, and $\Omega_\Lambda = 0.714$. At the NGC 1275 distance, $0''.1$ corresponds to 34.4 pc.

2. Observations and Data Analysis

2.1. The ALMA Data

The observations were done in ALMA Band 6 ($\lambda = 1.3$ mm) to cover the CO(2−1) line with 47 antennas on 2017 November 27. The maximum and minimum baseline lengths
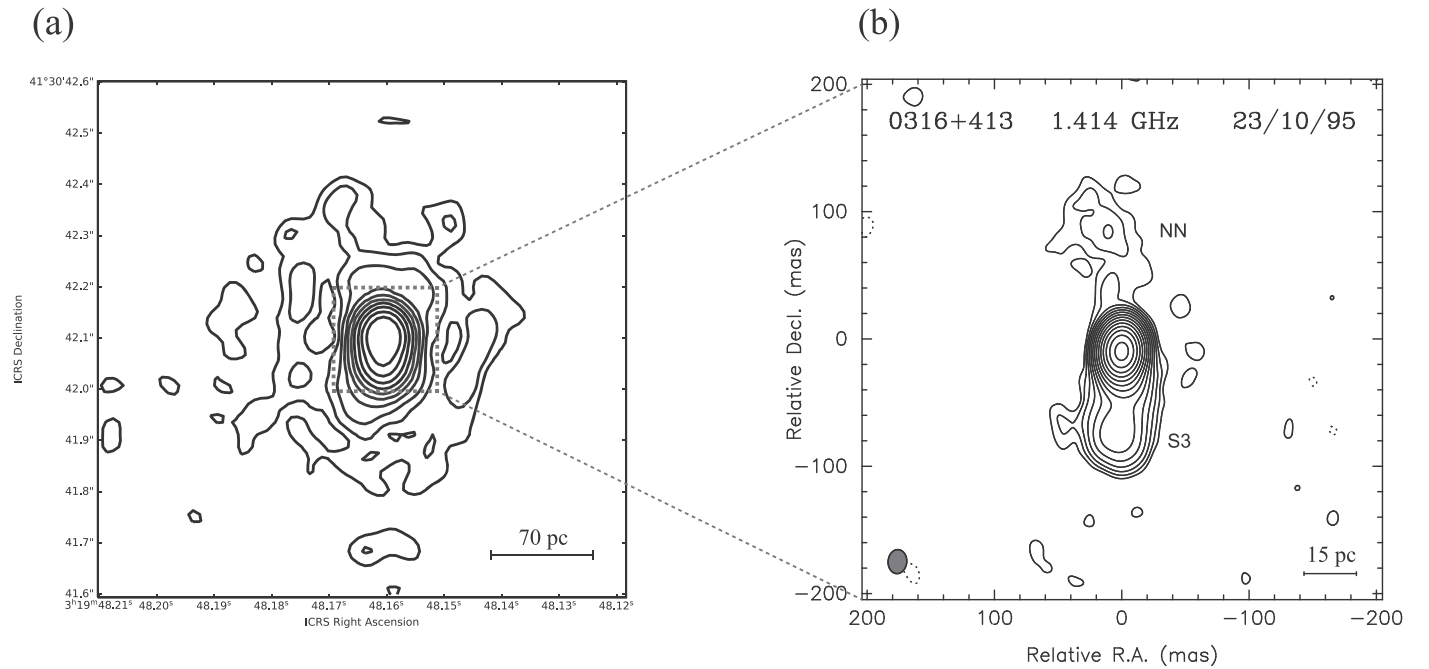
(a)

(b)

Figure 1. (a) Contours of the 330 MHz continuum image. The restoring beam is (46.6×39.8) mas at $4°.05$. The peak intensity is 2.5 Jy beam^{-1}. The contours are plotted at the level of $3\sigma \times (-1, 1, 2, 4, 8, 16, 32, 64, 128, 256, 512)$, where σ is the image noise rms of 0.573 mJy beam^{-1}. The gray broken square indicates the area of Figure 1(b). (b) Contours of the 1.4 GHz continuum image (Silver et al. 1998) that highlights the inner jet structure (© AAS. Reproduced with permission).

were 8.5 km and 92.1 m, respectively. The observations consisted of 52 scans with a 54.4 s integration for each scan bracketed by the scans for the observations of the complex gain calibrator. Integration time per interferometric visibility was set to 2 s. The data were processed at the East Asia ALMA Regional Center (EA-ARC) with a standard manner using the software CASA 5.1.1-5 and ALMA Pipeline version 40896. Images were created with a velocity resolution of 20 km s^{-1} with the "nearest" interpolation in frequency. Deconvolution was performed with the CLEAN algorithm using the CASA task `tclean` noninteractively. We performed self-calibration using the continuum emission of NGC 1275 in both phase and amplitude that improved the image quality significantly. The phase and amplitude self-calibration were done per integration time and per scan, respectively. Final image rms is 0.87 mJy beam^{-1} with natural weighting. The beam size is (144×77) mas at a position angle of $4°.0$. Further details on the observations and data analysis are provided in Nagai et al. (2019).

2.2. The VLBA Data

We analyzed archival Very Long Baseline Array (VLBA) data. The observation was carried out at 330 MHz with the 10 VLBA stations on 1995 October 23. The net integration time for NGC 1275 was 250 minutes. Standard data flagging, bandpass and amplitude calibrations, and fringe fitting were performed with the Astronomical Image Processing System (AIPS). Image deconvolution and self-calibration were performed using the software DIFMAP. We began self-calibration with a long solution interval and subsequently shortened the solution interval down to 1 minute. Figure 1 shows the CLEANed image. The image rms is 0.573 mJy beam^{-1} with natural weighting. The beam size is (47×40) mas at $4°$. The image was previously reported in Silver et al. (1998) and we

reproduced a consistent image in terms of its overall structure, the image noise rms, and the peak intensity.

3. Results

Figure 2 shows the 330 MHz continuum map overlaid on the velocity integrated map (moment 0) of the CO(2−1). The velocity integrated image of the CO(2−1) is the same image presented in Nagai et al. (2019). The image was created with natural weighting. The image shows a disk-like morphology with a radius of ∼100 pc. There are clumpy substructures within the disk that suggest its nonuniformity. Nagai et al. (2019) reported the velocity structure of the disk and found a velocity gradient along the position angle of ∼70°. This velocity gradient is most likely explained by the disk rotation. A similar morphology and velocity structure are also seen in the images of HCN(3−2) and HCO^{+}. More details about the properties of the molecular CND can be found in Nagai et al. (2019).

The continuum image at 330 MHz shows the diffuse emission (denoted "millihalo" in Silver et al. 1998) surrounding the central bright component. It has been reported that the central component appears to be dominated by the jet/lobe emission with a projected length of 30 pc at higher frequencies (Romney et al. 1995; Silver et al. 1998). The flux density of the diffuse emission is mostly below 10 mJy beam^{-1} (∼0.5% of the peak intensity). Silver et al. (1998) reported a power-law spectrum for the diffuse continuum emission, which demonstrates that it has a nonthermal origin. Remarkably, the diffuse continuum emission shows a good spatial coincidence with the molecular CND at 30–100 pc.

Absolute position information was lost due to the self-calibration for both the VLBA and ALMA images; thus, the center of the VLBA image may not be the same as that of the ALMA image. The center of the VLBA image must be the position where the 330 MHz emission is the strongest. This
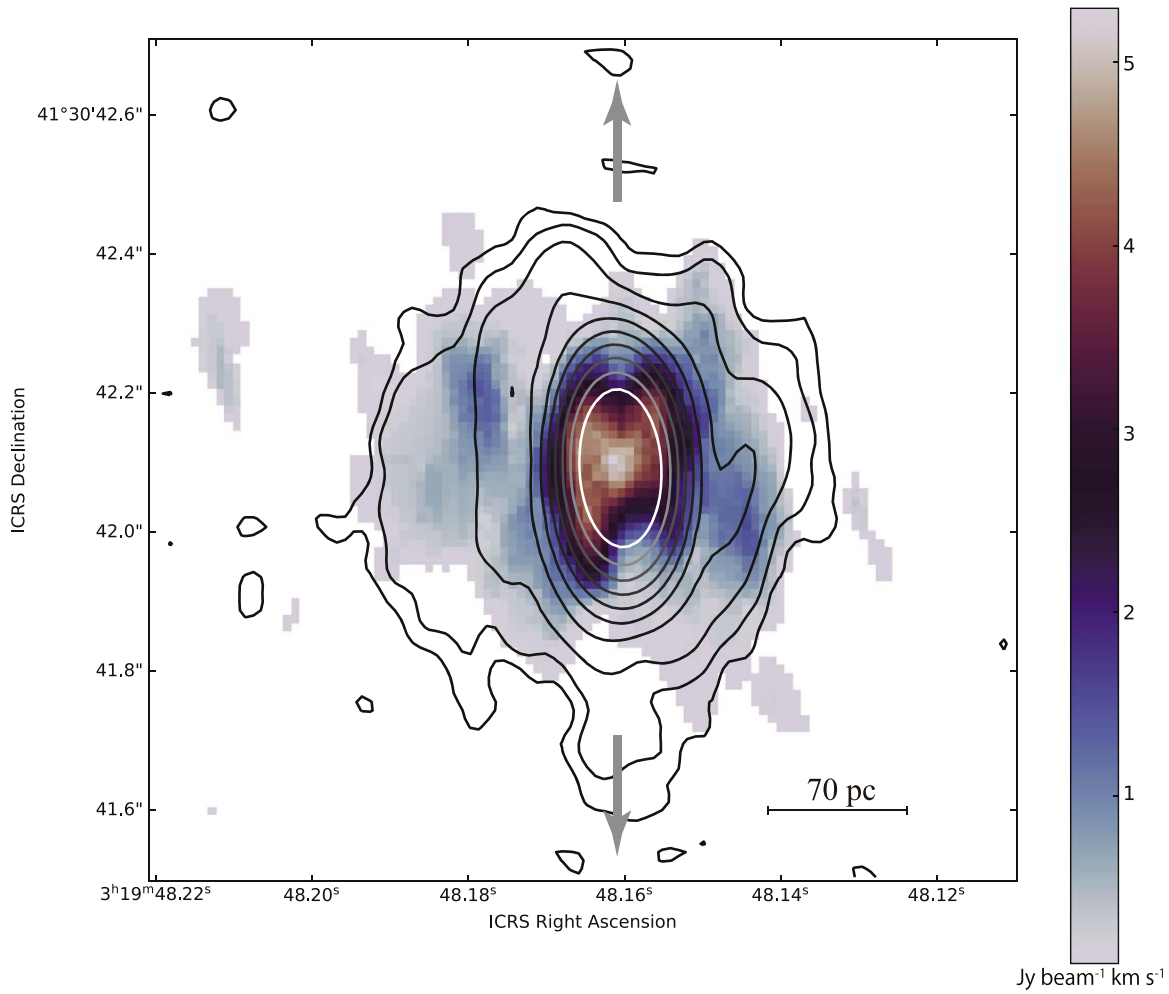
Figure 2. Contour map at 330 MHz intensity overlaid on the velocity integrated intensity (moment 0 map) of the CO(2−1) in color. The restoring beam of the CO(2−1) moment 0 map is (144 × 77) mas at 4°.0. The images are plotted throughout the region where the flux density of the image cube with a velocity resolution of 20 km s^{-1} is greater than 5σ (1σ = 0.87 mJy). The contour map is also convolved with the same restoring beam. The gray arrows in the north and south indicate an approximate direction of the jet shown in Figure 1(b).
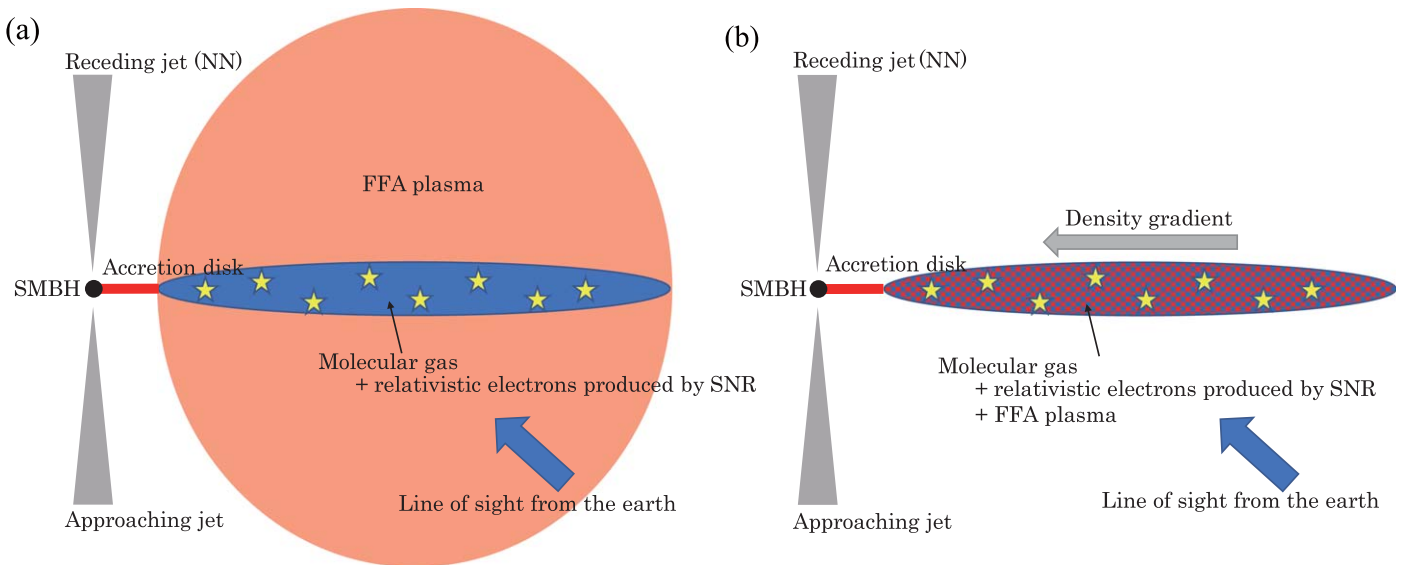

Figure 3. Schematic picture of possible CND structure. (a) The FFA plasma is more extended along the vertical direction than the molecular CND. The scale radius of the FFA plasma structure does not have to be the same, but it must be larger than ∼30 pc so that the plasma intercepts our line of sight to the receding jet (component NN in Figure 1). (b) The FFA plasma and molecular gas coexist within the same CND plane with density increase toward the SMBH.

position probably coincides with S1 (Silver et al. 1998), which is offset from the VLBI core by ~10 mas. The center of the ALMA image must coincide with the VLBI core where the millimeter continuum emission is expected to be the strongest (see the discussion in Nagai et al. 2017). This could result in a positional mismatch between the VLBA and ALMA images at a level of 10 mas. However, this level of offset is smaller than the size of the restoring beam. The spatial coincidence of the molecular CND with the 330 MHz synchrotron emission should be still watertight.

4. Discussion

4.1. Origin of the Diffuse Synchrotron Emission

The spatial coincidence of molecular CND with diffuse continuum emission indicates that both molecular gas and relativistic electrons are colocated in the same disk. What is the origin of the relativistic electrons? One possible answer is the relativistic electrons that are accelerated by the SN explosion, while another is those provided by the AGN.

The AGN of NGC 1275 shows prominent radio-jet activity (Nagai et al. 2010, 2014) that can supply the relativistic electrons. For the Fanaroff–Riley Type I (FRI) AGNs (Fanaroff & Riley 1974), jets gradually loosen their collimation as they propagate; as a result, the jets become wider at their downstream, but the overall structure generally maintains the two-sided shape that does not resemble the observed diffuse radio emission in NGC 1275. For the Fanaroff–Riley Type II (FRII) AGNs (Fanaroff & Riley 1974), the jets are well collimated up to the termination points (hotspots), and the shocked gas (relativistic electrons) leaks out therefrom. The sideway expansion of the shocked gas and propagation of the hotspots can make the overall structure a "cocoon" shape (Begelman & Cioffi 1989). One might think that the observed diffuse radio emission in NGC 1275 can be explained by the cocoon emission. However, the emission from the cocoon must be brighter on both sides of the hotspot and dimmer near the AGN because of the cooling of electrons by synchrotron radiation (e.g., Carilli et al. 1991). Furthermore, many FRII sources show that the cocoon is longer in the jet direction (Alexander & Leahy 1987) because the propagation speed of hotspots is faster than the speed of sideway expansion. Therefore, it seems to be difficult to explain the relatively symmetric shape and uniform brightness of the diffuse radio emission in NGC 1275 as shocked gas in the cocoon associated with the jets on a tens of parsec scale (shown in Figure 1(b)) or jets extending further out (Pedlar et al. 1990). In summary, the relativistic electrons carried by AGN jets cannot be the reason for the diffuse radio emission in NGC 1275.

Relativistic electrons that are produced near the jet base may be transported outward from the AGN. The transported electrons could propagate preferentially over the disk if the toroidal magnetic field was predominant in the disk. Silver et al. (1998) derived an Alfvén velocity of ~430 km s^{-1} using an equipartition magnetic field of 200 μG and gas density of 1 cm^{-3}. This gas density was derived using the equipartition condition between the relativistic plasma and the thermal gas pressures at a gas temperature of ~10^7 K (Fabian et al. 1981). It was concluded that the derived velocity was close to that required to supply relativistic electrons to the edge of the source within the electron cooling timescale of 3.2×10^5 yr at 330 MHz without requiring reacceleration. This can be true if only the hot plasma radiating X-ray emission at the core of the Perseus cluster is responsible for the gas pressure. However, the gas density should be much higher than the number used for the calculation by Silver et al. (1998) because of the presence of the molecular CND with a gas density of 10^3–10^4 cm^{-3} (Scharwächter et al. 2013; Nagai et al. 2019). Thus, the electrons cannot reach the edge of the CND. Therefore, the diffuse radio emission cannot originate from the AGN. The most likely origin is the relativistic electrons accelerated by the SN explosions in the CND.

Silver et al. (1998) reported that the radio luminosity of the CND shows a good agreement with the infrared luminosity as seen in normal galaxies (Condon 1992). The inferred SFR is 3 $M_\odot$ yr^{-1} (Silver et al. 1998; note that Silver et al. 1998 derived SFR = 6.4h^{-2} $M_\odot$ yr^{-1}, where $H_0 = 100h$ km s^{-1} Mpc^{-1}). We note that this SFR is consistent with that constrained by the observation of PAHs and far-infrared luminosity (SFR < 8.22 $M_\odot$ yr^{-1}: Oi et al. 2010). For the case of the Milky Way galaxy, a number of different observations suggest that the SN rate is about a hundredth of the SF rate (see Table 1 in Diehl et al. 2006). If we apply this relation to NGC 1275, ~10^4 of SNs should have happened within the electron cooling timescale. Higher angular resolution observations might be able to resolve individual SNs, as demonstrated in NGC 7469 (Colina et al. 2001) and Arp 220 (Lonsdale et al. 2006). It would also be important to resolve the CND by near-infrared continuum observations with the adoptive optics to obtain further confirmation of the SF activity in the CND.

4.2. Comparison with the SN-driven Turbulence Model

Kawakatu et al. (2020) provided a turbulent velocity (v_t) in the CND (see Equation (8) in Kawakatu et al. 2020) based on the SN-driven turbulence model, where the turbulence is driven by the energy input from the SN explosion. For NGC 1275, we take a molecular gas mass ($M_{\rm gas}$) of ~10^8 $M_\odot$ (Nagai et al. 2019), a star formation rate (SFR) of 3 $M_\odot$ yr^{-1} (Silver et al. 1998), a black hole mass ($M_{\rm BH}$) of 1×10^9 $M_\odot$ (Nagai et al. 2019), and a disk radius (r) of 100 pc (Nagai et al. 2019). Using these estimates, we obtain the following:

$$v_t = 24 \text{ km s}^{-1} \left[\frac{C_*}{3 \times 10^{-8} \text{ yr}^{-1}} \right]^{1/2}$$
$$\times \left[\frac{M_{\rm BH}}{10^8 M_\odot} \right]^{-1/4} \left[\frac{r}{100 \text{ pc}} \right]^{3/4}, \qquad (1)$$

where $C_* = {\rm SFR}/M_{\rm gas}$, which agrees well with the observed velocity dispersion of ~25 km s^{-1} on the ~100 pc scale of the CND (Nagai et al. 2019). This supports the idea that the SN explosion is the main driver of the turbulence in the CND.

Kawakatu et al. (2020) also gave the thickness of the CND. For the case of NGC 1275, Equation (9) in Kawakatu et al. (2020) can be written as

$$\frac{h(r_{\rm out})}{r_{\rm out}} \sim 0.08 \left[\frac{C_*}{3 \times 10^{-8} \text{ yr}^{-1}} \right]^{1/2}$$
$$\times \left[\frac{M_{\rm BH}}{10^8 M_\odot} \right]^{-3/4} \left[\frac{r_{\rm out}}{100 \text{ pc}} \right]^{5/4}, \qquad (2)$$

where $r_{\rm out}$ is the outer radius of the CND and $h(r_{\rm out})$ is the scale height of the disk at $r = r_{\rm out}$. Therefore, the CND of NGC 1275

is expected to be thin. This agrees with the signature of the low-covering fraction of fluorescent FeKα matter detected by X-ray observations (Hitomi Collaboration et al. 2018). With h ($r = 100$ pc) $\simeq 10$ pc, the dissipation timescale of the turbulence ($t_{\mathrm{dis}} = h/v_t$, see Kawakatu et al. 2020) is estimated to be 4×10^6 yr. About 10^5 SNs should have happened within this timescale if we take SFR $= 3\,M_\odot\,\mathrm{yr}^{-1}$ (Silver et al. 1998) and an SN rate of one-hundredth of the SF rate (Diehl et al. 2006). This indicates that the SN explosions must continuously supply the energy in the CND against the energy dissipation. Therefore, the diffuse synchrotron emission should not be the fossil of old SNs but young enough to account for the CO velocity dispersion.

We can also compare the black hole accretion rate derived from the observed bolometric luminosity with the accretion rate at the inner radius of the CND ($\dot{M}_{\mathrm{acc}}(r_{\mathrm{in}})$) predicted by the SN-driven turbulence model. Using Equation (8) in Izumi et al. (2016), we can write $\dot{M}_{\mathrm{acc}}(r_{\mathrm{in}})$ of NGC 1275 as

$$\left[\frac{\dot{M}_{\mathrm{acc}}(r_{\mathrm{in}})}{M_\odot\,\mathrm{yr}^{-1}}\right] \sim 3 \times 10^{-4} \left[\frac{r_{\mathrm{in}}}{3\,\mathrm{pc}}\right]^3 \left[\frac{r_{\mathrm{out}}}{100\,\mathrm{pc}}\right]^{-2}$$
$$\times \left[\frac{C_*}{3 \times 10^{-8}\,\mathrm{yr}^{-1}}\right] \left[\frac{M_{\mathrm{gas}}}{M_{\mathrm{BH}}}/0.1\right]. \qquad (3)$$

For simplicity, we have assumed that the gas is uniformly distributed over the CND. The observed bolometric luminosity is 4×10^{44} erg s^{-1}, which gives an accretion rate of 6×10^{-2} with a radiation efficiency of 0.1. Thus, the model-predicted accretion rate is approximately 3 orders of magnitude smaller than the black hole accretion rate inferred from the bolometric luminosity (4×10^{44} erg s^{-1}: Levinson et al. 1995). This might indicate the nonuniformity of the CND that results in a strong time variation of the accretion rate or additional mechanisms to enhance the turbulence, such as a more intense starburst, for the inner disk. It might also suggest that other channels of gas accretion, such as chaotic cold accretion (Gaspari et al. 2013), increase the black hole accretion rate.

Similar CND properties have been observed in the ultraluminous infrared galaxy (ULIRG) Mrk 231. Diffuse synchrotron emission around the AGN is observed in the central kiloparsec (Carilli et al. 1998; Taylor et al. 1999), which coincides spatially with the molecular CND (Bryant & Scoville 1996; Downes & Solomon 1998; Feruglio et al. 2015). Taylor et al. (1999) concluded that the diffuse synchrotron emission is most probably related to the star formation activity in the CND. Interestingly, the radio lobe/jet morphology is very similar to that of 3C 84 (the radio source of NGC 1275). Both sources show a pair of compact radio lobes/jets where the emission from the counterjet is free–free absorbed by the disk (Ulvestad et al. 1999). Using Equation (3), we obtain $\dot{M}_{\mathrm{acc}}(r_{\mathrm{in}}) \sim 6 \times 10^{-2}\,M_\odot\,\mathrm{yr}^{-1}$ for Mrk 231 with $r_{\mathrm{out}} = 200$ pc (Feruglio et al. 2015), SFR $= 220\,M_\odot\,\mathrm{yr}^{-1}$ (Taylor et al. 1999), $M_{\mathrm{gas}} \sim 10^9\,M_\odot$ (Downes & Solomon 1998), and $M_{\mathrm{BH}} \sim 10^8\,M_\odot$ (Kawakatu et al. 2007; Yan et al. 2015). This is somewhat smaller than the black hole accretion rate ($\sim 1.5\,M_\odot\,\mathrm{yr}^{-1}$) inferred from the bolometric luminosity of 10^{46} erg s^{-1} (Veilleux et al. 2009). Probing the star formation activity at the innermost CND region would be important to obtain a better estimate of the accretion rate for both NGC 1275 and Mrk 231 in the future.

4.3. The CND Structure

The emission from the northern jet (receding jet) should pass through the CND if the CND plane is perpendicular to the jet axis.[4] Silver et al. (1998) found that the integrated spectrum of the diffuse synchrotron emission from 330 MHz to 1.4 GHz is fairly straight in contrast to the curved spectrum of the northern jet component (labeled NN), which is located at a projected distance of ~ 35 pc ($\sim 0''1$) from the core. The curved spectrum likely indicates the free–free absorption (FFA). This difference in the spectral shape can provide insights into the structure of the CND. The free–free absorption opacity can be approximated as

$$\tau \approx 0.34 \left(\frac{T}{10^4\,\mathrm{K}}\right)^{-1.35} \left(\frac{\nu}{330\,\mathrm{MHz}}\right)^{-2.1}$$
$$\times \left(\frac{\mathrm{EM}}{10^4\,\mathrm{pc\,cm}^{-6}}\right), \qquad (4)$$

where T is the plasma temperature, ν is the observing frequency, and EM is the emission measure (Mezger & Henderson 1967). As the spectrum of the diffuse synchrotron emission is not significantly absorbed ($\tau < 1$) at a frequency down to 330 MHz, we obtain EM < 2.9 at $r \simeq 100$ pc with $T = 10^4$ K. On the other hand, component NN peaks at ~ 660 MHz in its spectrum (Silver et al. 1998). Thus, we obtain EM $= 12.7$ at $r_d = 35$ pc, where r_d is the projected distance of component NN from the core.

4.3.1. Vertical Stratification

Assuming that the electron density of the FFA plasma is uniform, we can ascribe the difference in EM to the difference in line-of-sight path length of the FFA plasma by a factor of $\gtrsim 4$. This can be realized if the plasma is extended spatially along the vertical direction and is shaped like a toroidal structure (Figure 3(a)).

Izumi et al. (2018) recently showed that the CND of the Circinus galaxy consists of the multiphase gas. They found that the diffuse atomic carbon (CI) is spatially extended more in the vertical direction of the disk than the dense molecular gas probed by the CO(3−2) emission, which is consistent with the radiation-driven fountain model (Wada 2012). For NGC 1275, the atomic phase gas in the high CND latitude may be ionized by the ultraviolet (UV) irradiation from young and luminous star clusters around the AGN (Richer et al. 1993), which then causes the FFA. Alternatively, the FFA plasma might originate in the ionized gas produced at the further inner part of the CND/accretion disk and be outflowed by the AGN radiation. There is evidence for such an ionized layer, with the lack of molecular gas, in the numerical simulations (Figure 1(c) in Wada et al. 2016). The ionized outflows have indeed been observed in the inner 500 pc of NGC 1275 by recent Gemini/NIFS observations (Riffel et al. 2020). On the other hand, the relativistic electrons supplied by SN remnants would accumulate in the midplane of the disk because the star formation activity in the CND is likely more efficient in the dense gas region.

---

[4] There are several estimates of the viewing angle of the jet (θ_{jet}). Here we assume that $\theta_{\mathrm{jet}} = 65° \pm 16°$ (Fujita & Nagai 2017).

4.3.2. Density Gradient in the CND

Alternatively, the observed difference in EM can be explained as if the molecular gas, nonthermal electrons, and FFA plasma are mixed in the same CND plane and their density becomes higher toward the inner radius of the CND (Figure 3(b)). In this case, FFA plasma is likely produced by the UV radiation from the stars in the CND.

We cannot discriminate between the two scenarios mentioned above with the present data. A spectral study of diffuse synchrotron emission with more resolution elements and greater sensitivity would help to improve our understanding of the distribution of the FFA matter in relation to the CND. Future high dynamic range observations with VLBI at $\lesssim$1GHz with the Square Killometer Array (SKA) and next-generation Very Large Array (ngVLA) or similar study of other AGNs would be useful for unveiling a more detailed picture of CNDs.

ORCID iDs

H. Nagai ⬤ https://orcid.org/0000-0003-0292-3645
N. Kawakatu ⬤ https://orcid.org/0000-0003-2535-5513

References

Alexander, P., & Leahy, J. P. 1987, MNRAS, 225, 1
Begelman, M. C., & Cioffi, D. F. 1989, ApJL, 345, L21
Bryant, P. M., & Scoville, N. Z. 1996, ApJ, 457, 678
Carilli, C. L., Perley, R. A., Dreher, J. W., et al. 1991, ApJ, 383, 554
Carilli, C. L., Wrobel, J. M., & Ulvestad, J. S. 1998, AJ, 115, 928
Colina, L., Alberdi, A., Torrelles, J. M., et al. 2001, ApJL, 553, L19
Combes, F., García-Burillo, S., Audibert, A., et al. 2019, A&A, 623, A79
Condon, J. J. 1992, ARA&A, 30, 575
Diehl, R., Halloin, H., Kretschmer, K., et al. 2006, Natur, 439, 45
Downes, D., & Solomon, P. M. 1998, ApJ, 507, 615
Fabian, A. C., Hu, E. M., Cowie, L. L., et al. 1981, ApJ, 248, 47
Fabian, A. C., Johnstone, R. M., Sanders, J. S., et al. 2008, Natur, 454, 968
Fanaroff, B. L., & Riley, J. M. 1974, MNRAS, 167, 31P
Feruglio, C., Fiore, F., Carniani, S., et al. 2015, A&A, 583, A99
Fujita, Y., & Nagai, H. 2017, MNRAS, 465, L94
Gaspari, M., Ruszkowski, M., & Oh, S. P. 2013, MNRAS, 432, 3401
Hitomi Collaboration, Aharonian, F., Akamatsu, H., et al. 2018, PASJ, 70, 13
Imanishi, M., Nakanishi, K., Izumi, T., & Wada, K. 2018, ApJL, 853, L25
Izumi, T., Kawakatu, N., & Kohno, K. 2016, ApJ, 827, 81
Izumi, T., Wada, K., Fukushige, R., et al. 2018, ApJ, 867, 48
Kawakatu, N., Imanishi, M., & Nagao, T. 2007, ApJ, 661, 660
Kawakatu, N., & Wada, K. 2008, ApJ, 681, 73
Kawakatu, N., Wada, K., & Ichikawa, K. 2020, ApJ, 889, 84
Levinson, A., Laor, A., & Vermeulen, R. C. 1995, ApJ, 448, 589
Lim, J., Ao, Y., & Dinh-V-Trung 2008, ApJ, 672, 252
Lonsdale, C. J., Diamond, P. J., Thrall, H., et al. 2006, ApJ, 647, 185
Mezger, P. G., & Henderson, A. P. 1967, ApJ, 147, 471
Nagai, H., Fujita, Y., Nakamura, M., et al. 2017, ApJ, 849, 52
Nagai, H., Haga, T., Giovannini, G., et al. 2014, ApJ, 785, 53
Nagai, H., Onishi, K., Kawakatu, N., et al. 2019, ApJ, 883, 193
Nagai, H., Suzuki, K., Asada, K., et al. 2010, PASJ, 62, L11
Oi, N., Imanishi, M., & Imase, K. 2010, PASJ, 62, 1509
Pedlar, A., Ghataure, H. S., Davies, R. D., et al. 1990, MNRAS, 246, 477
Peeters, E., Spoon, H. W. W., & Tielens, A. G. G. M. 2004, ApJ, 613, 986
Richer, H. B., Crabtree, D. R., Fabian, A. C., et al. 1993, AJ, 105, 877
Riffel, R. A., Storchi-Bergmann, T., Zakamska, N. L., et al. 2020, MNRAS, 496, 4857
Romney, J. D., Benson, J. M., Dhawan, V., et al. 1995, PNAS, 92, 11360
Salomé, P., Combes, F., Revaz, Y., et al. 2008, A&A, 484, 317
Scharwächter, J., McGregor, P. J., Dopita, M. A., & Beck, T. L. 2013, MNRAS, 429, 2315
Silver, C. S., Taylor, G. B., & Vermeulen, R. C. 1998, ApJ, 502, 229
Taylor, G. B., Silver, C. S., Ulvestad, J. S., et al. 1999, ApJ, 519, 185
Ulvestad, J. S., Wrobel, J. M., & Carilli, C. L. 1999, ApJ, 516, 127
Veilleux, S., Rupke, D. S. N., Kim, D.-C., et al. 2009, ApJS, 182, 628
Wada, K. 2012, ApJ, 758, 66
Wada, K., Schartmann, M., & Meijerink, R. 2016, ApJL, 828, L19
Walker, R. C., Dhawan, V., Romney, J. D., Kellermann, K. I., & Vermeulen, R. C. 2000, ApJ, 530, 233
Yan, C.-S., Lu, Y., Dai, X., et al. 2015, ApJ, 809, 117